


## Article

# Degradation of Tetracycline Hydrochloride by Cu-Doped MIL-101(Fe) Loaded Diatomite Heterogeneous Fenton Catalyst

Kang-Ping Cui <sup>1,\*</sup>, Yu-Ying He <sup>1</sup>, Kai-Jie Xu <sup>1</sup>, Yu Zhang <sup>2</sup>, Chang-Bin Chen <sup>3</sup>, Zheng-Jiang Xu <sup>3</sup>  
and Xing Chen <sup>1,2,\*</sup> 

<sup>1</sup> School of Resource and Environmental Engineering, Hefei University of Technology, Hefei 230009, China; heyuying131@163.com (Y.-Y.H.); XUKaijie@mail.hfut.edu.cn (K.-J.X.)

<sup>2</sup> Key Lab of Aerospace Structural Parts Forming Technology and Equipment of Anhui Province, Institute of Industry and Equipment Technology, Hefei University of Technology, Hefei 230009, China; zhangyu70714@163.com

<sup>3</sup> Anqing Shuguang Chemical Co., Ltd., Anqing 246003, China; chenchangbin19@163.com (C.-B.C.); xuzhengjiang19@163.com (Z.-J.X.)

\* Correspondence: cuikangping@hfut.edu.cn (K.-P.C.); xingchen@hfut.edu.cn (X.C.)

**Abstract:** In this work, the combination of high surface area diatomite with Fe and Cu bimetallic MOF material catalysts (Fe<sub>0.25</sub>Cu<sub>0.75</sub>(BDC)@DE) were synthesized by traditional solvothermal method, and exhibited efficient degradation performance to tetracycline hydrochloride (TC). The degradation results showed: Within 120 min, about 93% of TC was degraded under the optimal conditions. From the physical–chemical characterization, it can be seen that Fe and Cu play crucial roles in the reduction of Fe<sup>3+</sup> because of their synergistic effect. The synergistic effect can not only increase the generation of hydroxyl radicals (•OH), but also improve the degradation efficiency of TC. The Lewis acid property of Cu achieved the pH range of reaction system has been expanded, and it made the material degrade well under both neutral and acidic conditions. Loading into diatomite can reduce agglomeration and metal ion leaching, thus the novel catalysts exhibited low metal ion leaching. This catalyst has good structural stability, and less loss of performance after five reaction cycles, and the degradation efficiency of the material still reached 81.8%. High performance liquid chromatography–mass spectrometry was used to analyze the degradation intermediates of TC, it provided a deep insight of the mechanism and degradation pathway of TC by bimetallic MOFs. This allows us to gain a deeper understanding of the catalytic mechanism and degradation pathway of TC degradation by bimetallic MOFs catalysts. This work has not only achieved important progress in developing high-performance catalysts for TC degradation, but has also provided useful information for the development of MOF-based catalysts for rapid environmental remediation.

**Keywords:** Fenton-like catalyst; bimetallic MOF; diatomite; synergistic effect; antibiotics



**Citation:** Cui, K.-P.; He, Y.-Y.; Xu, K.-J.; Zhang, Y.; Chen, C.-B.; Xu, Z.-J.; Chen, X. Degradation of Tetracycline Hydrochloride by Cu-Doped MIL-101(Fe) Loaded Diatomite Heterogeneous Fenton Catalyst. *Nanomaterials* **2022**, *12*, 811. <https://doi.org/10.3390/nano12050811>

Academic Editor: Sónia Carabineiro

Received: 5 January 2022

Accepted: 25 January 2022

Published: 28 February 2022

**Publisher's Note:** MDPI stays neutral with regard to jurisdictional claims in published maps and institutional affiliations.



**Copyright:** © 2022 by the authors. Licensee MDPI, Basel, Switzerland. This article is an open access article distributed under the terms and conditions of the Creative Commons Attribution (CC BY) license (<https://creativecommons.org/licenses/by/4.0/>).

## 1. Introduction

In recent years, the problem of wastewater caused by antibiotics has been widely concerning. With the development of modern medicine, antibiotic pollution is becoming one of the water pollution problems faced by all humankind [1]. Because many antibiotics are not biodegradable and have strong chemical stability in water environments, the antibiotics in municipal wastewater especially cannot be completely removed, which endangers the safety of the ecosystem and causes great harm to human health [2,3]. The annual discharge of antibiotics in China exceeds 50,000 tons, and the ecological environment of most water bodies is seriously threatened. As a typical antibiotic, tetracycline hydrochloride is widely used in human and veterinary medicine [4,5]. Among different antibiotics, tetracycline hydrochloride (TC) occupies second place in production and usage, and has high antibacterial activity against a variety of pathogenic bacteria [6]. Therefore, it is important to explore

new techniques for the effective degradation of tetracycline, especially Fenton oxidation, for TC removal from wastewater.

At present, Fenton oxidation is the most-used method for wastewater with high antibiotic content. However, the traditional Fenton oxidation based on Ferrous ions ( $\text{Fe}^{2+}$ ) suffers from some serious drawbacks, including the production of large amounts of Fe sludge, a narrow pH range and exhibiting low reusability [7,8]. To address the shortcomings of homogeneous Fenton, a heterogeneous Fenton process using solids as catalysts was developed, such as  $\gamma\text{-FeOOH}/\text{GPCA}$  [9],  $\text{MnFe}_2\text{O}_4/\text{bio-char}$  [10], and  $\text{Fe}_3\text{O}_4/\text{SiO}_2$  [11].

Metal–organic frameworks (MOFs) are crystalline porous materials formed by the assembly of organic ligands and transition metal ions (or clusters). MOFs have developed rapidly in the past two decades and have impacted many fields, including separation [12], energy storage [13], sensing [14], and catalysis [15]. MOF materials have been widely used in catalysis over the past few decades due to their unique structure. MOFs have many useful properties, such as tunable porosity, interconnected pores, and large specific surface area. These properties facilitate the diffusion of pollutants and products during catalytic reactions. Fe-based MOFs (Fe-MOFs) have received particular attention over the past few decades [16,17]. Compared with other metal catalysts, Fe is non-toxic and the second-most productive metal. Although some other transition metals (such as Co [18]) have been gradually applied to heterogeneous Fenton catalysts, the high toxicity and high application cost of these metals make the Fe-based heterogeneous catalysts stand out from other catalysts.

In recent years, it has also been noticed that when a second metal ion invades the framework nodes, the catalytic performance of MOFs can be improved [19]. Bimetallic catalysts have excellent catalytic performance because of the increased specific surface area of the material or the synergistic effect between metals, which also provides additional reaction sites for  $\text{H}_2\text{O}_2$  activation. Due to the good compatibility of MOFs with various metal centers (such as Fe, Cu, Co, and Zn), some MOFs can have both metal centers and bind to organic ligands [20,21], thus the catalytic activity of heterogeneous reaction was improved. For example, Qiao Sun et al. first described partial substitution of Fe in Fe-(BDC) metal–organic frameworks with Mn, Co, and Ni. The results show that the addition of Mn can significantly improve the degradation efficiency [22]. Bimetallic Fenton catalysts prepared by using MOF materials as precursors or templates have better catalytic performance than traditional preparation methods. Some researchers have synthesized  $\text{CoMn}_2\text{O}_4$  microporous plates using MOFs as precursors. Compared with  $\text{CoMn}_2\text{O}_4$  synthesized by the traditional solvothermal method, this catalyst has a higher specific surface area and abundant  $\bullet\text{OH}_{\text{surf}}$ . It also has higher catalytic activity [23]. The results show that the use of bimetallic MOFs as efficient Fenton-like catalysts is a promising approach.

Because the redox potential of  $\text{Cu}^{2+}/\text{Cu}^+$  ( $E_0 = 0.17\text{ V}$ ) is lower than  $\text{Fe}^{3+}/\text{Fe}^{2+}$  ( $E_0 = 0.77\text{ V}$ ),  $\text{Cu}^+$  has a stronger reducibility than  $\text{Fe}^{2+}$ . Meanwhile, the interfacial electron transfer can be accelerated through the interaction between the two metal redox pairs of Fe and Cu, thereby improving the catalytic performance of  $\text{H}_2\text{O}_2$  activation [24]. In particular, the Cu has Lewis acid properties, which can interact with Fe species to form a local acidic microenvironment, and expand the pH range of the system [25]. Modification of pristine MIL-101(Fe) with copper as the second metal component and optimized the proportions of Fe and Cu metal elements.

In addition, the activity and stability of the catalyst decreases due to the inevitable metal leaching and agglomeration of nanoparticles [26]. In addition to doping non-metallic elements [27,28], fixing the MOFs in the core–shell [29,30] or loading it on the macromolecular carrier [16,31] can also reduce the leaching of metal ions and make the metal ions disperse and not agglomerate easily. Diatomite (DE) is a naturally-occurring porous mineral with a complex three-dimensional (3D) structure [32]. Acid treatment may increase the surface area and pore size by eliminating impurities responsible for pore blockage [33]. DE has good adsorption performance and is a highly promising potential carrier material candidate for heterogeneous Fenton catalysts. Using DE as the carrier of the metal catalyst can

decrease their aggregation effect and thus improve the catalytic activity [34]. Simultaneously, the stability of the catalyst can also be improved by reducing the leaching of metal ions [16].

In this study,  $\text{Fe}_{0.25}\text{Cu}_{0.75}(\text{BDC})@\text{DE}$  was fabricated and used as a Fenton-like catalyst to degrade TC in a solution. Above all, the ratio of Fe and Cu was optimized, and the catalyst reached a high level of degradation. Then the optimal ratio of the catalyst was loaded onto diatomite to reduce agglomeration and metal ion leaching. Finally, through detailed characterization of the composite catalyst, including the morphology, composition, and other structural properties of the catalyst, the stability and cyclability of the catalyst and the possible catalytic mechanism and TC degradation pathway were elucidated.

## 2. Experimental

### 2.1. Materials and Chemicals

The chemicals used in this work were iron (III) chloride hexahydrate ( $\text{FeCl}_3 \cdot 6\text{H}_2\text{O}$ ), copper nitrate trihydrate ( $\text{Cu}(\text{NO}_3)_2 \cdot 3\text{H}_2\text{O}$ ), sulfuric acid ( $\text{H}_2\text{SO}_4$ ), and potassium iodide (KI), all acquired from Sinopharm Chemical Reagent Co., Ltd., Shanghai, China. Terephthalic acid ( $\text{H}_2\text{BDC}$ ), anhydrous ethanol ( $\text{C}_2\text{H}_5\text{OH}$ ), tetracycline hydrochloride (TC-HCl), *p*-Benzoquinone (BQ), and tertiary butanol (TBA) were supplied from Shanghai Maclin Chemistry Co., Ltd., Shanghai, China. Hydrogen peroxide ( $\text{H}_2\text{O}_2$ ), *N,N*-dimethylformamide (DMF), and sodium hydroxide (NaOH), were purchased from Shanghai Aladdin Chemistry Co., Ltd., Shanghai, China. Diatomite (DE) was purchased from International Building Materials Environmental Technology Co., Ltd., Shanghai, China.

### 2.2. Preparation of Catalysts

#### 2.2.1. Synthesis of $\text{Fe}_x\text{Cu}_y(\text{BDC})$

Fe and Cu bimetallic MOF composites were produced via a facile solvothermal method. In a traditional synthesis, the required number of  $\text{FeCl}_3 \cdot 6\text{H}_2\text{O}$  and  $\text{Cu}(\text{NO}_3)_2 \cdot 3\text{H}_2\text{O}$  was added to 30 mL of DMF solution, and then 5 mmol  $\text{H}_2\text{BDC}$  (0.830 g) was dissolved in 30 mL DMF of solution under magnetic stirring. After mixing the two solutions and continuing the magnetic stirring for half an hour at room temperature, the solutions were poured into a 100 mL Teflon-lined stainless-steel autoclave (Lichen, Shanghai, China), and the temperature was maintained at 110 °C for 36 h under autogenous pressure for a solvothermal reaction. After natural cooling, the resulting precipitates were collected and washed with DMF, ethanol, and deionized water to remove residual impurities, and dried at 80 °C for 12 h. The total molar amount of  $\text{FeCl}_3 \cdot 6\text{H}_2\text{O}$  and  $\text{Cu}(\text{NO}_3)_2 \cdot 3\text{H}_2\text{O}$  used to synthesize the samples was fixed at 10 mmol. The resultant samples were denoted as  $\text{Fe}_{0.75}\text{Cu}_{0.25}(\text{BDC})$ ,  $\text{Fe}_{0.5}\text{Cu}_{0.5}(\text{BDC})$ , and  $\text{Fe}_{0.25}\text{Cu}_{0.75}(\text{BDC})$ , separately. For comparison with bimetallic MOFs, two monometallic samples containing only  $\text{FeCl}_3 \cdot 6\text{H}_2\text{O}$  and  $\text{Cu}(\text{NO}_3)_2 \cdot 3\text{H}_2\text{O}$  were prepared: Fe(BDC) and Cu(BDC). Table 1 records the parameters of all sample synthesis.

**Table 1.** Synthetic parameters of all prepared samples.

Sample	N ( $\text{FeCl}_3 \cdot 6\text{H}_2\text{O}$ ) (mmol)	N ( $\text{Cu}(\text{NO}_3)_2 \cdot 3\text{H}_2\text{O}$ ) (mmol)	N ( $\text{FeCl}_3 \cdot 6\text{H}_2\text{O}$ )/n( $\text{Cu}(\text{NO}_3)_2 \cdot 3\text{H}_2\text{O}$ )
Fe(BDC)	10.0	0	-
$\text{Fe}_{0.75}\text{Cu}_{0.25}(\text{BDC})$	7.5	2.5	3:1
$\text{Fe}_{0.5}\text{Cu}_{0.5}(\text{BDC})$	5	5	1:1
$\text{Fe}_{0.25}\text{Cu}_{0.75}(\text{BDC})$	2.5	7.5	1:3
Cu(BDC)	0	10.0	-

#### 2.2.2. Synthesis of Fe-Cu Bimetallic MOF@DE

Fe-Cu bimetallic MOF@DE were produced using the same operations procedures, the solution was mixed, and 1 g of DE was added and magnetic stirring continued for 1 h. It was then poured into a 100 mL Teflon-lined stainless-steel autoclave, and the temperature was maintained at 110 °C for 36 h under autogenous pressure for a solvothermal reaction.

### 2.3. Characterization of Catalysts

The specific surface morphology of all the prepared samples were obtained by SU-8020 scanning electron microscopy (SEM; Hitachi, Tokyo, Japan) and JEM-2100F transmission electron microscopy (TEM; JEOL, Tokyo, Japan). The crystalline structures of the prepared samples were recognized by powder X-ray diffraction (XRD) measurements (PANalytical, Almelo, The Netherlands). The XRD patterns were documented in the  $2\theta$  range of  $5\text{--}90^\circ$  with a scan rate of  $0.06^\circ \text{ min}^{-1}$  working at 40 kV and 40 mA. The nitrogen adsorption–desorption isotherm at 77 K was used to analyze the specific surface area and pore size distribution of samples by the Brunauer–Emmett–Teller (BET) analysis (Autosorb-IQ3, Quantachrome, Boynton Beach, FL, USA). Fourier transform infrared (FTIR) spectra was recorded by KI suppression disk technique in the  $4000\text{--}400 \text{ cm}^{-1}$  wave number range with a resolution of  $2 \text{ cm}^{-1}$  (KQ-300DE, Thermo, Waltham, MA, USA). The chemical valence states of the elements contained in the sample were detected by X-ray photoelectron spectroscopy (XPS, Shimadzu, Kyoto, Japan).

### 2.4. Catalytic Degradation Experiments

The reaction was added to a 100 mL sealed serum bottle with 50 mL of 20 mg/L TC solution, 0.5 M NaOH, and  $\text{H}_2\text{SO}_4$ , which was used to adjust the initial pH value. The samples was then placed in a constant temperature shaker table (200 rpm,  $25^\circ\text{C}$ ) for adsorption to reach equilibrium after 30 min.  $\text{H}_2\text{O}_2$  was then added for a Fenton-like degradation reaction. During the reaction, 1 mL of the solution was collected at given time intervals and filtered to remove solid impurities. After quenching with excess tert-butanol, the absorbance of the pollutant was tested at 375 nm using an ultraviolet spectrophotometer. For the recycling measurement, the catalyst was collected by centrifugation, the material washed until neutral, and then dried.

The stock solution of TC was prepared with a concentration of 1 g/L, diluted to different concentrations, and its standard curve was measured. The mother liquor was diluted to the corresponding concentration and we checked whether its concentration was accurate every time the degradation experiment was performed to ensure that the TC was not photolyzed.

### 2.5. Analytical Methods

TC contents were measured by ultraviolet spectrophotometer (UV-Vis; Hitachi, Tokyo, Japan). We detected the dynamic change of absorbance in the wavelength range during the reaction was 200–450 nm. The degradation intermediates of TC were assayed by high performance liquid chromatography–mass spectrometry (HPLC-MS; Water, Williamsburg, VA, USA). The mobile phase was a mixture of acetonitrile and oxalic acid (20:80, *v/v*) with a flow rate of 1.0 mL/min. Total organic carbon (TOC) was analyzed by using a TOC/TN analyzer (Multi N/C 2100, Analytik Jena AG Corporation, Jena, Germany). The amount of leached Fe and Cu ions in the solution after the reaction were detected by atomic absorption spectroscopy (AAS; AA140, VARIAN, Crawley, UK).  $\bullet\text{OH}$  radicals were detected with 50 mM DMPO as the scavenger using electron paramagnetic resonance spectroscopy (ESR; Bruker, Bremen, Germany).

## 3. Results and Discussion

### 3.1. Characterization of Catalysts

The crystal information and chemical composition of the samples prepared with different ratios of Fe and Cu were analyzed by XRD. Figure 1 showed the XRD spectra of Fe and Cu ratios of 1:0, 3:1, 1:1, 1:3, and 0:1, respectively. For the diffraction peak of Cu-free doped catalyst, the value of the obvious peak is consistent with the diffraction peak of MIL-101 (Fe) previously reported [35]. When Cu is added into the catalyst, the ratio of Fe to Cu becomes 3:1. The diffraction peak of the sample has no significant difference, indicating that adding small amounts of Cu to the catalyst did not affect the type of material produced, but the existence of Cu complexes is undeniable. Then the doping amount of Cu continues

to increase and the ratio of Fe to Cu becomes 1:1, 1:3, and 0:1, and the diffraction peaks among the three have no obvious difference. The main diffraction peaks of Cu(BDC) were basically consistent with those reported before [36]. After being doped with Cu, the XRD spectra of the four bimetallic samples are similar to MIL-101(Fe), indicating that Cu was successfully incorporated into the MIL-101(Fe). After doping the catalyst with the optimal ratio and diatomite, it can be seen from the diffraction peaks in the figure that the crystal structure of the sample has changed after adding Cu, so the XRD characterization results are also different. Different catalyst materials can be obtained by adjusting different ratio of Fe and Cu, and the degree to the left is less than  $1^\circ$ .

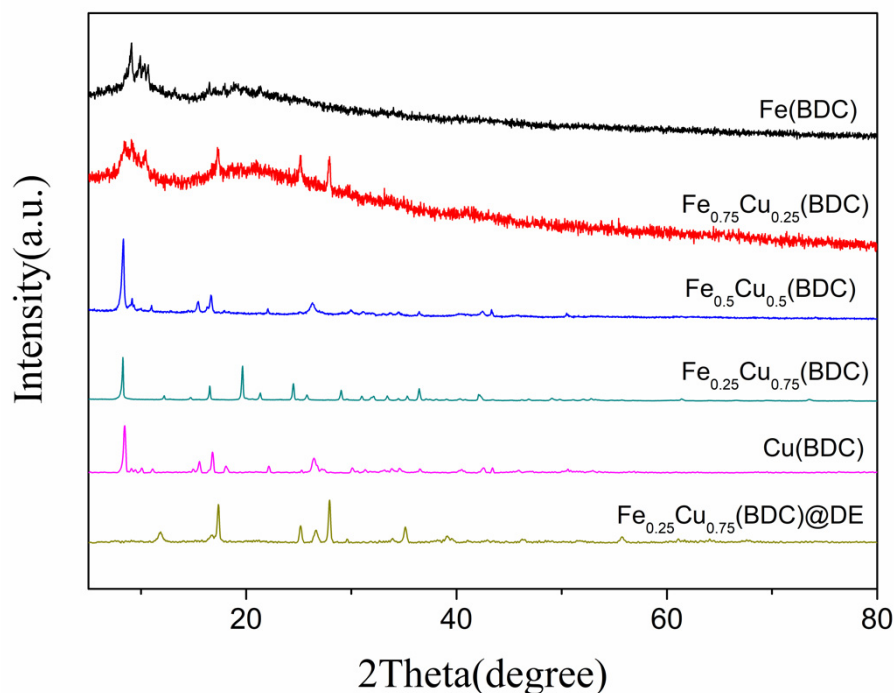


**Figure 1.** XRD patterns of Fe(BDC),  $\text{Fe}_{0.75}\text{Cu}_{0.25}$ (BDC),  $\text{Fe}_{0.5}\text{Cu}_{0.5}$ (BDC),  $\text{Fe}_{0.25}\text{Cu}_{0.75}$ (BDC), Cu(BDC), and  $\text{Fe}_{0.25}\text{Cu}_{0.75}$ (BDC)@DE.

The morphological structures and microstructures of the prepared samples were observed by SEM and TEM. Through SEM analysis, the morphological structures of these prepared samples were discerned. The FESEM image of Fe(BDC) exhibits an octahedral crystallite structure, while Cu(BDC) shows the presence of a cubic layered structure [37]. As shown in Figure 2a, there is disintegration of the original octahedral morphology into small irregular particles due to the introduction of Cu into the MIL-101(Fe) framework. It showed that  $\text{Fe}_{0.25}\text{Cu}_{0.75}$ (BDC) grew in a two-dimensional direction, forming irregular sheet-like structures. DE shows the perforated regular disc morphology (Figure 2c,d). It can be seen in (Figure 2b) where the  $\text{Fe}_{0.25}\text{Cu}_{0.75}$ (BDC) decorated on the DE surfaces results to form  $\text{Fe}_{0.25}\text{Cu}_{0.75}$ (BDC)@DE composite materials. From the TEM images (Figure 2e,f), the  $\text{Fe}_{0.25}\text{Cu}_{0.75}$ (BDC) were uniformly distributed. Simultaneously, the TEM showed  $\text{Fe}_{0.25}\text{Cu}_{0.75}$ (BDC)@DE: these components of Cu and Fe were equally formed on the DE surface. Furthermore, the SEM elemental mapping of  $\text{Fe}_{0.25}\text{Cu}_{0.75}$ (BDC)@DE revealed that these components of Fe, C, and O were uniformly formed on the surface (Figure S1).

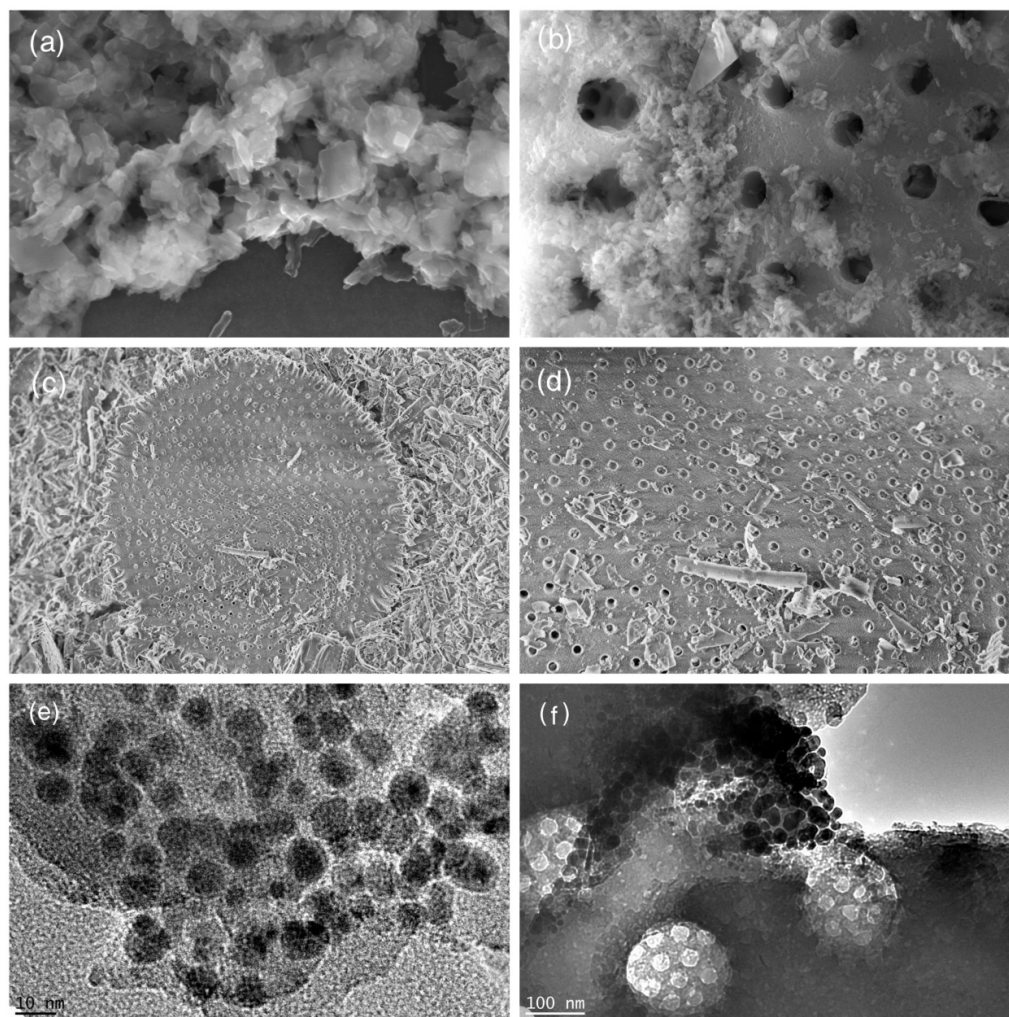


**Figure 2.** SEM images of  $\text{Fe}_{0.25}\text{Cu}_{0.75}(\text{BDC})$  (a),  $\text{Fe}_{0.25}\text{Cu}_{0.75}(\text{BDC})@\text{DE}$  (b) and DE (c,d); TEM images of  $\text{Fe}_{0.25}\text{Cu}_{0.75}(\text{BDC})$  (e),  $\text{Fe}_{0.25}\text{Cu}_{0.75}(\text{BDC})@\text{DE}$  (f).

Figure 3a displayed FT-IR spectrum of these synthesized catalysts. The O-H stretching vibration of water molecules adsorbed on the catalyst surface forms a broad band centered at  $3430\text{ cm}^{-1}$ . Characteristic peaks at  $1570$  and  $1393\text{ cm}^{-1}$  are due to carboxylate vibration. The characteristic absorption bands at  $1090\text{ cm}^{-1}$  and  $796\text{ cm}^{-1}$  can be attributed to the asymmetric stretching vibration and symmetric stretching vibration of the Si-O-Si bond [38], respectively. The stretching vibration of Fe-O corresponds to  $542\text{ cm}^{-1}$ , while the characteristic peak at  $569\text{ cm}^{-1}$  belongs to the Cu-O stretching vibration mode [21]. After the synthesis of the two metals at the same time, the wide peak is offset to  $560\text{ cm}^{-1}$ , which further proves the formation of bimetallic catalyst.

Figure 3b shows the nitrogen adsorption–desorption isotherms and pore size distributions of the composite catalysts. At moderate relative pressures (from 0.2 to 0.9), the  $\text{N}_2$  uptake of the catalyst samples gradually increases, indicating the presence of mesopores in the catalyst structure. The Fe(BDC) sample has higher microporosity because it exhibits significant  $\text{N}_2$  uptake at lower relative pressures (below 0.05) [37]. With the incorporation of Cu, the catalyst changes from micropores to mesopores, and the nanopore collapse is caused by the incorporation of Cu. The  $\text{Fe}_{0.25}\text{Cu}_{0.75}(\text{BDC})$  and DE surface areas were severally  $41.24\text{ m}^2/\text{g}$  and  $37.13\text{ m}^2/\text{g}$ . After doping, the specific surface areas of the composites were reduced to  $30.81\text{ m}^2/\text{g}$ , which further proved that  $\text{Fe}_{0.25}\text{Cu}_{0.75}(\text{BDC})$  was supported with DE (Table 2). The DFT pore size distribution curve also showed that the pore size

of the composite catalyst was distributed in both mesoporous and microporous, but both were smaller than that of  $\text{Fe}_{0.25}\text{Cu}_{0.75}(\text{BDC})$  and DE.

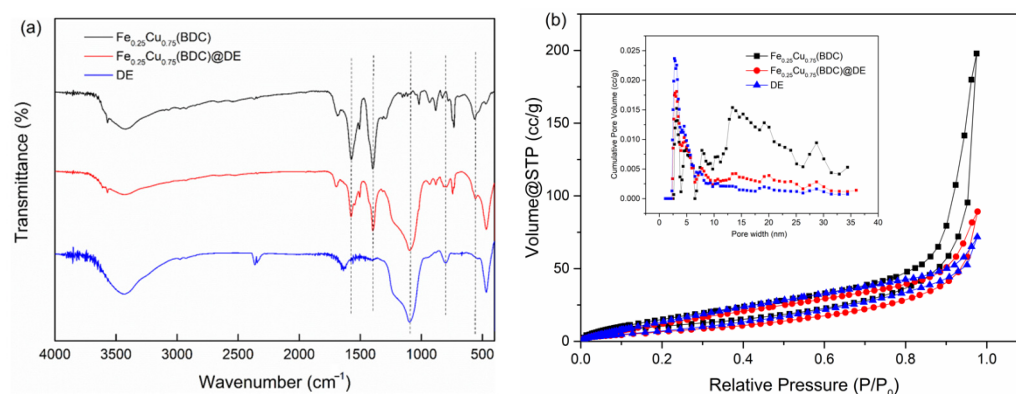


**Figure 3.** (a) FTIR spectra of  $\text{Fe}_{0.25}\text{Cu}_{0.75}(\text{BDC})$ ,  $\text{Fe}_{0.25}\text{Cu}_{0.75}(\text{BDC})@DE$ , DE and (b)  $\text{N}_2$  adsorption–desorption isotherms and pore size distribution plots of  $\text{Fe}_{0.25}\text{Cu}_{0.75}(\text{BDC})$ ,  $\text{Fe}_{0.25}\text{Cu}_{0.75}(\text{BDC})@DE$ , DE.

**Table 2.** Textural properties and total pore capacity of  $\text{Fe}_{0.25}\text{Cu}_{0.75}(\text{BDC})$ ,  $\text{Fe}_{0.25}\text{Cu}_{0.75}(\text{BDC})@DE$ , DE.

Sample	$S_{\text{BET}}$ ( $\text{m}^2/\text{g}$ )	Total Pore Volume ( $\text{cm}^3/\text{g}$ )	Average Pore Diameter (nm)
DE	37.13	0.11	59.84
$\text{Fe}_{0.25}\text{Cu}_{0.75}(\text{BDC})$	41.24	0.31	29.69
$\text{Fe}_{0.25}\text{Cu}_{0.75}(\text{BDC})@DE$	30.81	0.14	17.92

The chemical states of Cu and Fe on the composite catalyst surface can be studied by XPS survey. As observed from Figure 4a, four peaks at 711.0, 712.9, 724.6, and 726.5 eV in XPS spectra, assigned to  $\text{Fe}^{2+} 2p_{3/2}$ ,  $\text{Fe}^{3+} 2p_{3/2}$ ,  $\text{Fe}^{2+} 2p_{1/2}$ , and  $\text{Fe}^{3+} 2p_{1/2}$ , indicating that the composite catalyst is composed of  $\text{Fe}^{2+}$  and  $\text{Fe}^{3+}$  species [25]. In the Cu2p diagram (Figure 4b), four peaks are fitted at 933.2, 934.8 eV, 953.0, and 954.6 eV, corresponding to  $\text{Cu}^+ 2p_{3/2}$ ,  $\text{Cu}^{2+} 2p_{3/2}$ ,  $\text{Cu}^+ 2p_{1/2}$ , and  $\text{Cu}^{2+} 2p_{1/2}$ , which are the characteristic peaks of  $\text{Cu}^{2+}$  and  $\text{Cu}^+$  species [39]. The kinetic energy (KE) peaks in Figure 4c are 915.6 eV and 917.6 eV, corresponding to  $\text{Cu}^+$  and  $\text{Cu}^{2+}$ , respectively. The results further illustrate that the Cu species on the surface of  $\text{Fe}_{0.25}\text{Cu}_{0.75}(\text{BDC})$  and  $\text{Fe}_{0.25}\text{Cu}_{0.75}(\text{BDC})@DE$  samples mainly exist in the form of  $\text{Cu}^{2+}$  and  $\text{Cu}^+$ . The results show that the polyvalent states of Fe ( $\text{Fe}^{2+}$  and  $\text{Fe}^{3+}$ ) and Cu ( $\text{Cu}^+$  and  $\text{Cu}^{2+}$ ) coexist in composite catalyst. The survey spectra for  $\text{Fe}_{0.25}\text{Cu}_{0.75}(\text{BDC})$  and  $\text{Fe}_{0.25}\text{Cu}_{0.75}(\text{BDC})@DE$  were also assessed by the characteristic elements such as trace amount of C 1s and major elements O 1s and Si 2p scan (Figure S2).

### 3.2. Catalytic Performance of Catalysts

According to the adjustment of different ratios of Fe and Cu, the optimal ratio of Fe and Cu is selected as shown in Table 1, and then the catalyst with the optimal ratio is loaded onto diatomite to reduce the agglomeration of materials and the leaching of metal ions. The degradation efficiencies of five different Fe/Cu ratio catalysts at an initial TC concentration of 20 mg/L were compared in the  $\text{Fe}_x\text{Cu}_{1-x}(\text{BDC})/\text{H}_2\text{O}_2$  system (Figure 5). Almost no TC removal was observed when  $\text{H}_2\text{O}_2$  was added alone, revealing that the contribution of  $\text{H}_2\text{O}_2$  auto-oxidation is negligible. Simultaneously, the catalyst was first added to the TC solution for 30 min to achieve equilibrium of adsorption, and then  $\text{H}_2\text{O}_2$  was added for Fenton-like reaction. As displayed in Figure 5, after 30 min of adsorption equilibrium, the degradation effect of  $\text{Fe}_{0.25}\text{Cu}_{0.75}(\text{BDC})$  reached more than 50% at the 5 min, which was far greater than that of the other four catalysts. After 60 min, the removal efficiency of  $\text{Fe}_{0.25}\text{Cu}_{0.75}(\text{BDC})$ ,  $\text{Fe}(\text{BDC})$ , and  $\text{Fe}_{0.75}\text{Cu}_{0.25}(\text{BDC})$  was more than 90%. The

removal efficiency of Cu(BDC) and  $\text{Fe}_{0.5}\text{Cu}_{0.5}(\text{BDC})$  to degraded TC is only 10% and 60%, respectively. In addition, As the Cu content increases, the pore size distribution of  $\text{Fe}_{0.25}\text{Cu}_{0.75}(\text{BDC})$  changes from micropore to mesopore, which may be due to the collapse of nano-pore caused by Cu incorporation [37].

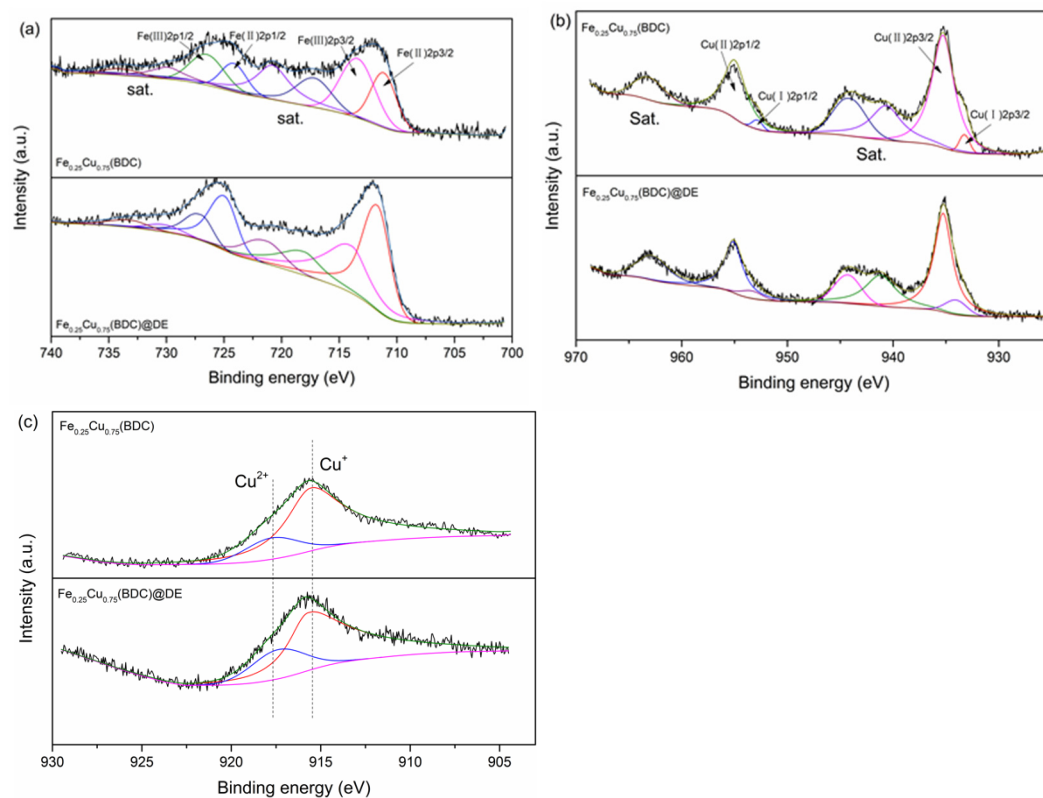


**Figure 4.** (a) Fe 2p XPS spectra, (b) Cu 2p XPS spectra, and (c) Cu LMM XPS spectra of  $\text{Fe}_{0.25}\text{Cu}_{0.75}(\text{BDC})$  and  $\text{Fe}_{0.25}\text{Cu}_{0.75}(\text{BDC})@DE$ .

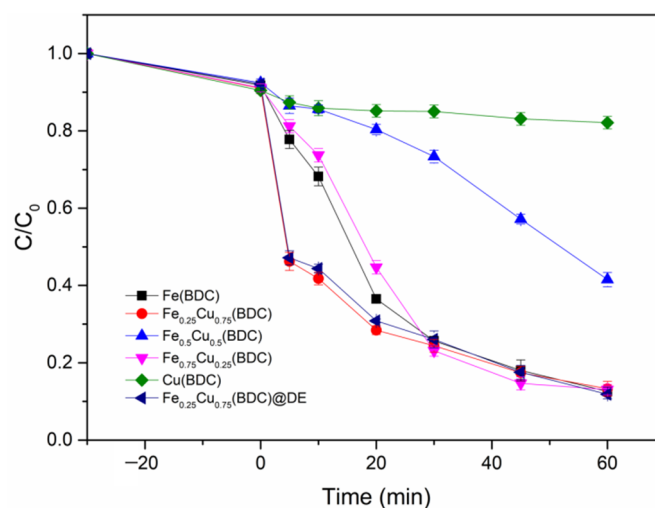


**Figure 5.** Degradation of TC by bimetallic MOFs prepared with different ratios of Fe and Cu and DE loaded MOF were compared (Experiment conditions:  $[\text{TC}] = 20 \text{ mg/L}$ ,  $[\text{catalyst}] = 0.6 \text{ g/L}$ ,  $[\text{H}_2\text{O}_2] = 10 \text{ mM}$ ,  $\text{pH} = 3$ ,  $T = 25 \text{ }^\circ\text{C}$ ).

The enlarged pore structure will facilitate the transfer and contact of reactants to the internal reaction site, and the appropriate pore distribution provides ideal permeability. At the same time, Cu has the property of Lewis acid, which can generate a local acidic



microenvironment through interaction with Fe species, thus improving the degradation efficiency of the material. In addition, the reason for the improved catalytic activity might be that the addition of Cu promotes the formation of Fe in the  $\text{Fe}_x\text{Cu}_{1-x}(\text{BDC})$  structure. The interfacial electron transfer can be accelerated by the interaction between the redox pair of Fe and Cu, thus improving the performance of the catalyst to activate  $\text{H}_2\text{O}_2$ . After increasing the amount of Cu, the pore structure collapse leads to a significant reduction in the specific surface area of the material, resulting in a limited number of active sites for activation of  $\text{H}_2\text{O}_2$ . With the increase of Cu doping, Lewis acids of Cu accounted for most of the influence, which also explained why the material degraded 50% TC within 5 min.

In order to reduce the aggregation of MOFs and the leaching problem of metal ions, the catalyst material with the best degradation effect can be loaded on the diatomite. It can be seen from Figure 6 that the degradation effect of the catalyst has reached more than 80% after the material is loaded on diatomite for 1 h of catalytic reaction. Even though the content of metal and the leaching of metal ions in  $\text{Fe}_{0.25}\text{Cu}_{0.75}(\text{BDC})@\text{DE}$  are less than those in  $\text{Fe}_{0.25}\text{Cu}_{0.75}(\text{BDC})$ , it has no effect on the removal effect of the catalyst. This further proves that the heterogeneous Fenton reaction plays a dominant role.

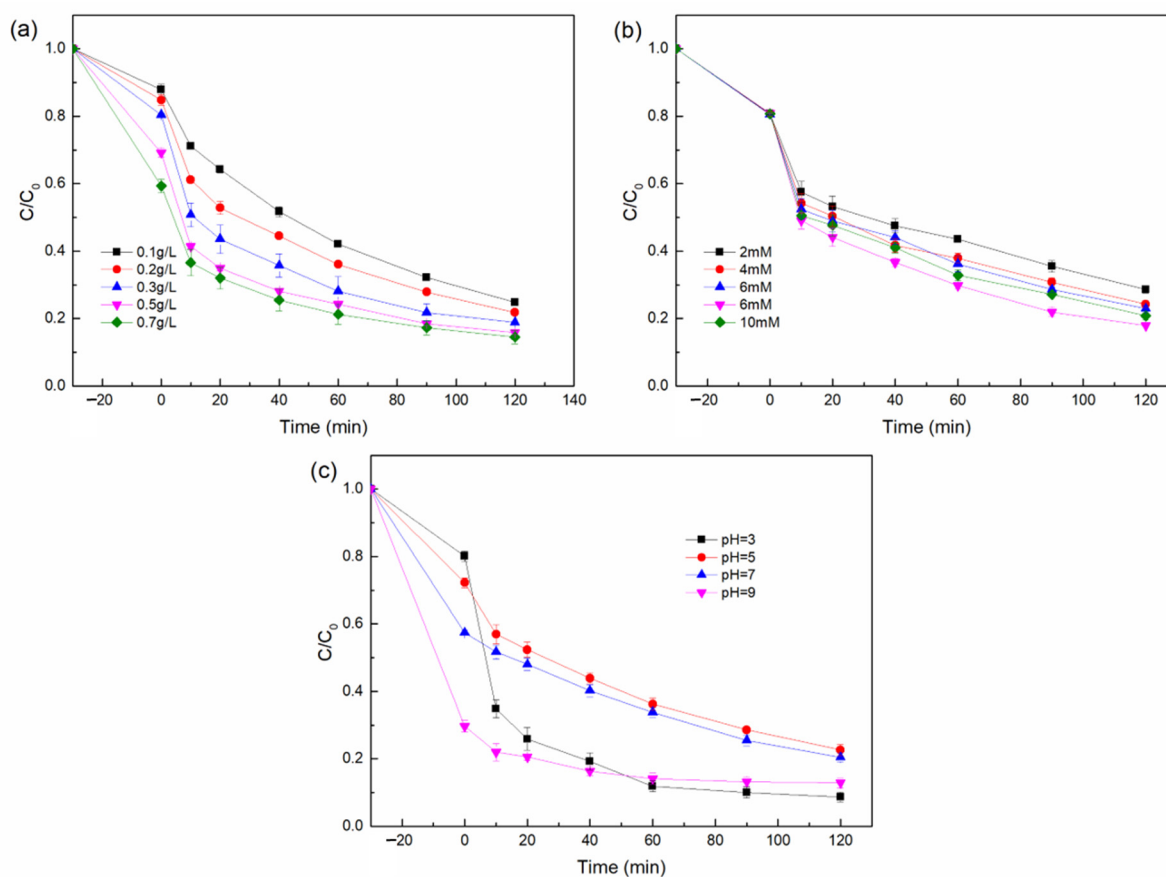


**Figure 6.** Influence factor experiments: effects of (a) catalyst dosage, (b)  $\text{H}_2\text{O}_2$  concentration, and (c) initial pH. Except for the investigated parameter, the others were fixed:  $[\text{TC}] = 20 \text{ mg/L}$ ,  $[\text{catalyst}] = 0.5 \text{ g/L}$ ,  $[\text{H}_2\text{O}_2] = 8 \text{ mM}$ ,  $\text{pH} = 7$ ,  $T = 25 \text{ }^\circ\text{C}$ .

To optimize the experimental conditions, we further researched the effects of pH,  $\text{H}_2\text{O}_2$  concentration, and catalyst dosage on the removal effect of TC by the composite catalyst. As the catalyst loading increased from 0.1 g/L to 0.7 g/L, the degradation rate of TC increased from 74.7 to 86.9%. This may be related to the increase of active sites activated by  $\text{H}_2\text{O}_2$ . From Figure 6a, with the catalyst dosage increasing, the removal rate of the contaminants was augmented. However, when the catalyst dosage was increased from 0.5 g/L to 0.7 g/L, the rate of removal efficiency slowed down. This was a result

of the aggregation of nanoparticles and diffusion limitation at higher concentrations of catalyst [40]. Therefore, 0.5 g/L was the optimum catalyst dosage and was chosen for further experiments.

As shown in Figure 6b, the degradation effect was significantly enhanced when the  $\text{H}_2\text{O}_2$  concentration was increased from 2 mM to 8 mM. TC removal rate increased from 70.6 to 87.2% when hydrogen peroxide dosage increased to 0.6 mM. This is probably due to the higher  $\text{H}_2\text{O}_2$  dosage which could be activated by the composite catalyst and generate more  $\bullet\text{OH}$  radicals to degrade TC. Nevertheless, in further increasing the  $\text{H}_2\text{O}_2$  dosage to 10 mM, the TC removal efficiency was reduced which was probably owing to the excessive  $\text{H}_2\text{O}_2$  causing the self-scavenger effect of  $\bullet\text{OH}$  radicals (Equations (1) and (2)) [21,41]. Thus, the optimum dosage of  $\text{H}_2\text{O}_2$  was 8 mM.

It is well acknowledged that initial pH value has a significant effect on the surface charge, existing form, stability of the catalyst, etc. [17]. Therefore, the influence of the initial pH with the range from 3 to 9 on the degradation of TC were investigated and the results are shown in Figure 6c. When the pH is 3, the removal efficiency of TC is 93.0%, which is consistent with the high removal efficiency of heterogeneous Fenton under extremely acidic conditions. When the pH is 9, the removal efficiency of TC also reaches 91.3%, but it is related to the adsorption properties of DE. Under alkaline conditions, the adsorption effect of DE is better. However, the adsorption effect of alkaline conditions is not conducive to the reuse of materials. When the pH is 5 and 7, the removal efficiency of TC also reaches about 80%, indicating that the material has a good degradation effect on TC under acidic and neutral conditions, which greatly expands the removal range of the pH. This may be due to the Lewis acid effect of Cu, leading to the formation of a small range of acidic environments, improving the degradation efficiency of the catalyst.



### 3.3. Reusability and Stability of Catalyst

From the point of view of the economic field, it is important to investigate the reusability and stability of catalysts. To examine the maintained catalytic capacity of the composite catalyst, the degradation of TC was conducted for five consecutive cycles. After each reaction, the catalyst was filtered and washed to neutral and dried, then put into the system for reuse. As shown in Figure 7,  $\text{Fe}_{0.25}\text{Cu}_{0.75}(\text{BDC})@\text{DE}$ 's degradation efficiency to TC remained at 81.8% after five consecutive cycles, proving that it has good catalytic stability.

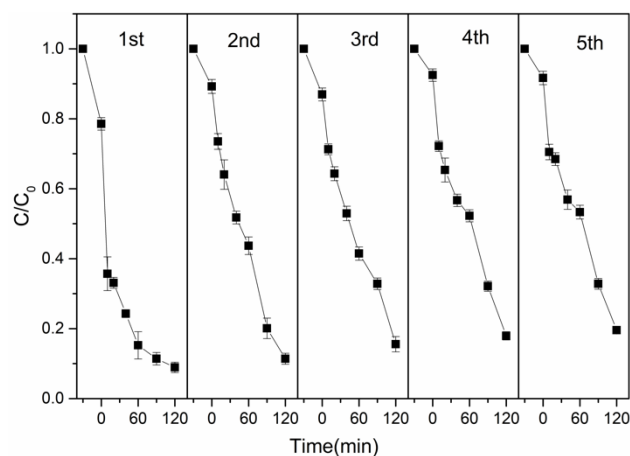


**Figure 7.** Recyclability of  $\text{Fe}_{0.25}\text{Cu}_{0.75}(\text{BDC})@\text{DE}$  on the degradation of TC. (Experiment conditions: pH = 3, [TC] = 20 mg/L, [Catalyst] = 0.5 g/L, [ $\text{H}_2\text{O}_2$ ] = 8 mM, T = 25 °C).

The high TC removal over  $\text{Fe}_{0.25}\text{Cu}_{0.75}(\text{BDC})@\text{DE}$  in the first round of catalytic reactions is partly related to its excellent adsorption capacity, which allows intermediates to be adsorbed on its surface during the catalytic reaction. TOC degradation efficiency within 30 min was 60%, and the removal efficiencies of TOC remained at a high level. To further demonstrate the stability of the composite catalyst, we further measured the total Fe and Cu leaching amounts in the solution. After 120 min of reaction, the concentration of total Cu satisfied the water environment discharge standards (2 mg/L) applied by the European Union, and no Fe element was found when tested in the solution.

There, the loss of catalyst activity may be due to the coverage of active sites, the accumulation of residual TC and intermediates on the catalyst surface, as well as the leakage of Cu ions from the catalyst.

### 3.4. Identification of Radicals

A spin-trapping electron paramagnetic resonance (EPR) technique and radical quenching experiments were employed to help identify free radicals generated in Fenton-like catalytic reaction systems. Quenching experiments were performed with quenchers (t-butanol (TBA) (scavenger for all  $\bullet\text{OH}$ ), p-benzoquinone (p-BQ) (scavenger for  $\bullet\text{O}_2^-$ ), and potassium iodide (KI) (scavenger for surface-bound radical  $\bullet\text{OH}$ )) to determine the free radicals contributing to TC degradation. It can be seen from Figure 8a that the removal rate of TC decreased from 91.9% to 30.1% and 38.8% within 120 min after excessive addition of tert-Butanol and KI, respectively. It is proved that the degradation of TC is mainly related to the surface-bound  $\bullet\text{OH}$  radicals, but not to the free  $\bullet\text{OH}$  radicals, and the heterogeneous Fenton reaction played a dominant role. In addition, when excessive BQ ( $\bullet\text{O}_2^-$  radicals inhibitor) was added, the removal rate of TC decreased slightly from 91.9% to 85.5%, indicating that  $\cdot\text{O}_2$  might be involved in the degradation of TC.

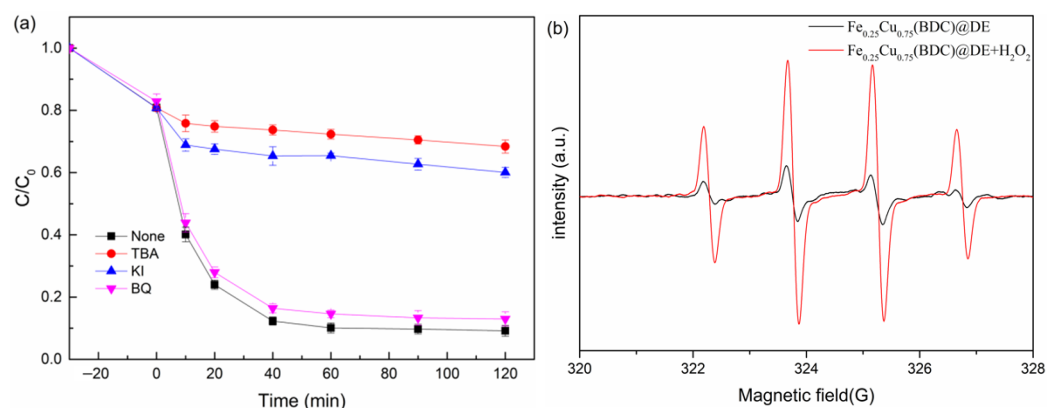


**Figure 8.** (a) Effect of radical scavengers on the degradation of TC. (b) ESR spectra of DMPO- $\text{OH}\cdot$  adducts that formed over time with Fenton-like degradation. (Experiment conditions:  $[\text{TC}] = 20 \text{ mg/L}$ ,  $[\text{H}_2\text{O}_2] = 8 \text{ mM}$ ,  $[\text{catalyst}] = 0.5 \text{ g/L}$ ,  $[\text{BQ}] = 10 \text{ mM}$ ,  $[\text{TBA}] = 100 \text{ mM}$ ,  $[\text{KI}] = 10 \text{ mM}$ ).

For EPR tests, the spin trapping agent was DMPO ( $\bullet\text{OH}$ ), as the EPR spectrum picture shows (Figure 8b). In the ESR technique of  $\text{Fe}_{0.25}\text{Cu}_{0.75}(\text{BDC})@\text{DE} / \text{H}_2\text{O}_2$  system, the  $\bullet\text{OH}$  radical has four adsorption peaks with as intensity ratio of 1:2:2:1, while there is no obvious characteristic peak in the DMPO system. The results further showed that  $\bullet\text{OH}$  radicals were formed on the catalyst surface.

### 3.5. Reaction Pathway of TC Degradation

The degradation intermediates of TC were measured by HPLC-MS, based on this information and relevant literature [42,43]. The possible degradation pathway is presented in Figure 9. It has been observed that nine meaningful products were identified with peaks of  $m/z$  309,  $m/z$  324,  $m/z$  384,  $m/z$  249,  $m/z$  229,  $m/z$  283,  $m/z$  176,  $m/z$  131, and  $m/z$  146 (Figure S3). Initially, the main characteristic peak of TCH ( $m/z = 445$ ) was detected before

degradation [44]. There are two main reasons for the generation of these intermediates throughout the Fenton-like degradation process: loss of functional groups and open-loop reactions. First, TCH ( $m/z = 445.0$ ) was transformed into P1 ( $m/z = 309$ ), P2 ( $m/z = 324$ ), and P3 ( $m/z = 384$ ). These products were mainly derived from dihydroxylation, demethylation, dehydration, and deamination products [45]. Next, the intermediates with the P4 ( $m/z = 249$ ), P5 ( $m/z = 229$ ) and P6 ( $m/z = 283$ ) were formed due to the ring-opening reactions and the cleavage of carbon bond [46]. With further oxidation, the product with P7 ( $m/z = 176$ ), P8 ( $m/z = 131$ ), P9 ( $m/z = 146$ ) were formed through bond cleavage, and finally some of them were completely degraded to  $\text{CO}_2$  and  $\text{H}_2\text{O}$  [47].

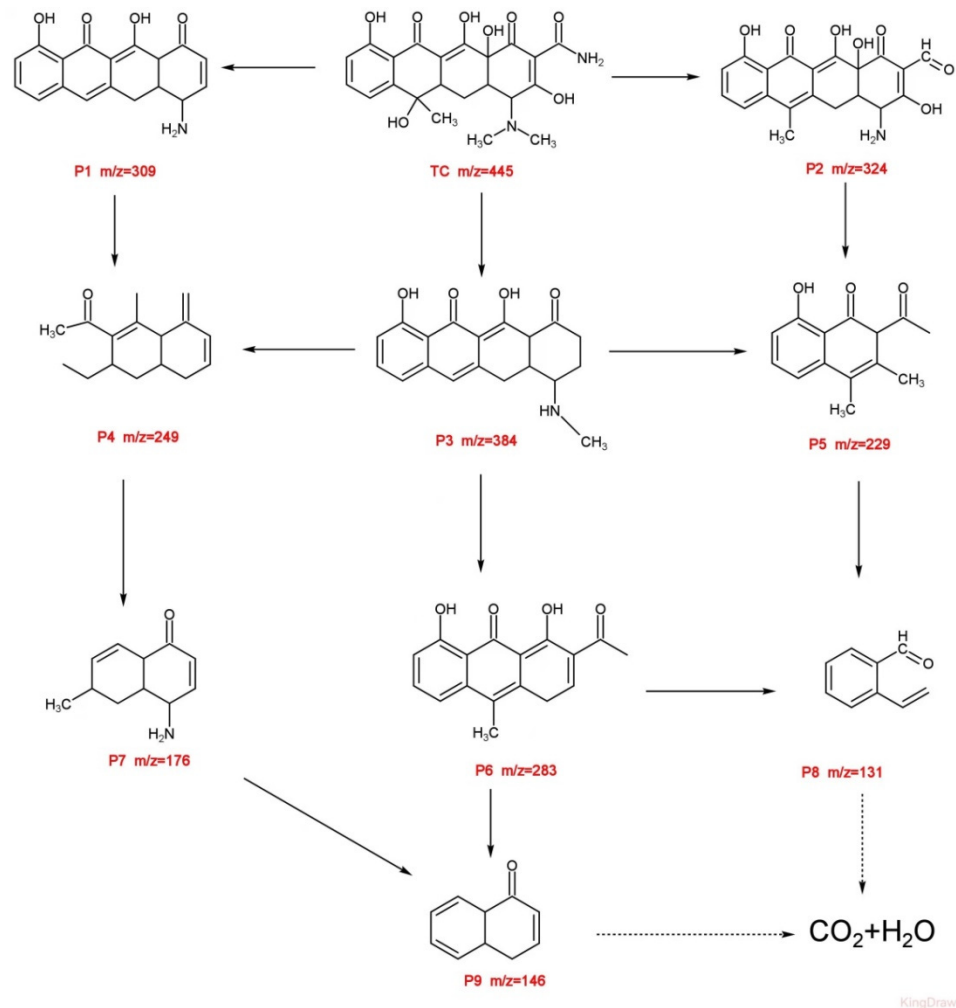
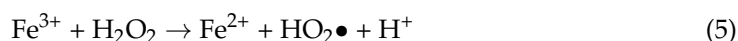
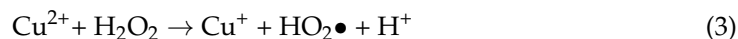


**Figure 9.** Proposed degradation pathways of TC in the  $\text{Fe}_{0.25}\text{Cu}_{0.75}(\text{BDC})@\text{DE} / \text{H}_2\text{O}_2$  system.

Based on the above analysis, the dominant free radicals were confirmed and a possible mechanism of TC degradation mechanism for this heterogeneous Fenton system was proposed. Firstly, TC is adsorbed from the bulk solution to the catalyst surface via the  $\pi-\pi$  interaction between the benzene rings of TC and mesoporous DE. Then, once  $\text{H}_2\text{O}_2$  is added, the metal ions on the catalyst surface combine with surface-coordinated  $\text{H}_2\text{O}_2$  to initiate heterogeneous Fenton reaction. Finally, the TC molecules are attacked by  $\bullet\text{OH}_{\text{surf}}$  radicals and mineralized into small molecular substances.

The main active substances are  $\text{Fe}^{2+}$  and  $\text{Cu}^+$  in activating  $\text{H}_2\text{O}_2$  to produce hydroxyl  $\bullet\text{OH}$ .  $\text{Cu}^+$  and  $\text{Fe}^{2+}$  are first reduced to  $\text{Cu}^+$  and  $\text{Fe}^{2+}$  on the catalyst surface by the captured electron from surface-coordinated  $\text{H}_2\text{O}_2$  (Equations (3) and (5)). Meanwhile,  $\text{Cu}^+$  and  $\text{Fe}^{2+}$  lost electrons to activate  $\text{H}_2\text{O}_2$  to generate  $\bullet\text{OH}$  and  $\text{Cu}^{2+}$  and  $\text{Fe}^{3+}$  (Equations (4) and (6)). Furthermore, the standard reduction potentials of Cu ( $E_0(\text{Cu}^{2+}/\text{Cu}^+) = 0.17 \text{ V}$ ) are

smaller than Fe ( $E_0(\text{Fe}^{3+}/\text{Fe}^{2+}) = 0.77\text{ V}$ ),  $\text{Cu}^+$  could promote the regeneration of  $\text{Fe}^{2+}$  through a thermodynamically profitable electron transfer process (Equation (7)). It can further promote the redox cycles of  $\text{Cu}^+/\text{Cu}^{2+}$  and  $\text{Fe}^{2+}/\text{Fe}^{3+}$  in catalysts, and maintain the formation of  $\bullet\text{OH}_{\text{surf}}$ . Thus, the effective cyclic conversion of  $\text{Fe}^{2+}/\text{Fe}^{3+}$  and  $\text{Cu}^+/\text{Cu}^{2+}$  guarantees the continuous activation of  $\text{H}_2\text{O}_2$  until it is completely consumed.



#### 4. Conclusions

We explored catalytic materials by adjusting different proportions of Fe and Cu metal elements via a facile solvothermal method. The bimetallic catalyst was then loaded on the DE to improve the stability of the catalyst, and it was used to activate  $\text{H}_2\text{O}_2$  to degrade TC.  $\text{Fe}_{0.25}\text{Cu}_{0.75}(\text{BDC})@\text{DE}/\text{H}_2\text{O}_2$ . The composite showed good catalytic performance, and the removal efficiency of TC was up to 93.0% within 120 min. Under the condition of ensuring the reusability of this catalyst, it can work efficiently in a wide pH range, and in acidic and neutral conditions. Cu has a Lewis acid effect, can form local acidic microenvironment, and can act synergically with Fe as the active site of  $\text{H}_2\text{O}_2$ . In addition, the degradation efficiency of the catalyst still reached 81.8% after five cycles, indicating that the catalyst has satisfactory reusability and minimal leaching of metal ions. Therefore, the stability, reusability, and high reactivity of the catalyst make it a promising application. It is possible for bimetallic MOFs to be used in the field of water remediation as pH-resistant Fenton catalysts.

**Supplementary Materials:** The following supporting information can be downloaded at: <https://www.mdpi.com/article/10.3390/nano12050811/s1>. Figure S1. (a) EDXS elemental mapping for  $\text{Fe}_{0.25}\text{Cu}_{0.75}(\text{BDC})@\text{DE}$  confirmed the presence of (b) C, (c) O (d) Si (e) Fe and (f) Cu.; Figure S2. (a) XPS survey spectrum and high-resolution XPS spectra of (b) C 1p, (c) O 1s for the  $\text{Fe}_{0.25}\text{Cu}_{0.75}(\text{BDC})$  and  $\text{Fe}_{0.25}\text{Cu}_{0.75}(\text{BDC})@\text{DE}$  nanoparticles, and (d) Si 2p. for  $\text{Fe}_{0.25}\text{Cu}_{0.75}(\text{BDC})@\text{DE}$  nanoparticles.; Figure S3. Mass spectrum of TC and its degradation intermediates.

**Author Contributions:** Conceptualization, K.-P.C. and X.C.; methodology, Y.Z.; validation, Y.-Y.H.; resources, C.-B.C. and Z.-J.X.; data curation, Y.-Y.H.; writing—original draft preparation, Y.-Y.H.; writing—review and editing, K.-J.X. and X.C.; supervision, K.-P.C. and X.C.; funding acquisition, K.-P.C. and X.C. All authors have read and agreed to the published version of the manuscript.

**Funding:** This research was funded by [the National Key R&D Program of China] grant number [2019YFC0408500], [Major Science and Technology Projects of Anhui Province] grant number [201903a07020009, 202003a07020004], [Hefei independent innovation policy loan transfer subsidy project] grant number [J2020K07]. And The APC was funded by [202003a07020004].

**Data Availability Statement:** Not applicable.

**Acknowledgments:** The authors thank the National Key R&D Program of China (2019YFC0408500), Major Science and Technology Projects of Anhui Province (201903a07020009, 202003a07020004), Hefei independent innovation policy loan transfer subsidy project (J2020K07) for financial support.

**Conflicts of Interest:** The authors declare no conflict of interest.

## References

1. Guo, R.X.; Liu, H.W.; Yang, K.; Wang, S.T.; Sun, P.P.; Gao, H.; Chen, F.J. beta-Cyclodextrin Polymerized in Cross-Flowing Channels of Biomass Sawdust for Rapid and Highly Efficient Pharmaceutical Pollutants Removal from Water. *Acs Appl. Mater. Interfaces* **2020**, *12*, 32817–32826. [[CrossRef](#)] [[PubMed](#)]
2. Cai, M.M.; Ma, S.T.; Hu, R.Q.; Tomberlin, J.K.; Yu, C.; Huang, Y.P.; Zhang, J.B. Systematic characterization and proposed pathway of tetracycline degradation in solid waste treatment by *Hermetia illucens* with intestinal microbiota. *Environ. Pollut.* **2018**, *242*, 634–642. [[CrossRef](#)] [[PubMed](#)]
3. Kummerer, K. Antibiotics in the aquatic environment—A review—Part II. *Chemosphere* **2009**, *75*, 435–441. [[CrossRef](#)] [[PubMed](#)]
4. Wang, S.L.; Wang, H. Adsorption behavior of antibiotic in soil environment: A critical review. *Front. Environ. Sci. Eng.* **2015**, *9*, 565–574. [[CrossRef](#)]
5. Zhao, R.Y.; Sun, X.X.; Jin, Y.R.; Han, J.S.; Wang, L.; Liu, F.S. Au/Pd/g-C<sub>3</sub>N<sub>4</sub> nanocomposites for photocatalytic degradation of tetracycline hydrochloride. *J. Mater. Sci.* **2019**, *54*, 5445–5456. [[CrossRef](#)]
6. Dai, W.D.; Jiang, L.; Wang, J.; Pu, Y.J.; Zhu, Y.F.; Wang, Y.X.; Xiao, B.B. Efficient and stable photocatalytic degradation of tetracycline wastewater by 3D Polyaniline/Perylene diimide organic heterojunction under visible light irradiation. *Chem. Eng. J.* **2020**, *397*, 125476. [[CrossRef](#)]
7. Xu, L.J.; Wang, J.L. Magnetic Nanoscaled Fe<sub>3</sub>O<sub>4</sub>/CeO<sub>2</sub> Composite as an Efficient Fenton-Like Heterogeneous Catalyst for Degradation of 4-Chlorophenol. *Environ. Sci. Technol.* **2012**, *46*, 10145–10153. [[CrossRef](#)]
8. Liu, Y.; Wang, J.L. Reduction of nitrate by zero valent iron (ZVI)-based materials: A review. *Sci. Total Environ.* **2019**, *671*, 388–403. [[CrossRef](#)]
9. Wang, Y.Z.; Zhang, H.M.; Li, B.K.; Yu, M.C.; Zhao, R.; Xu, X.T.; Cai, L. gamma-FeOOH graphene polyacrylamide carbonized aerogel as air-cathode in electro-Fenton process for enhanced degradation of sulfamethoxazole. *Chem. Eng. J.* **2019**, *359*, 914–923. [[CrossRef](#)]
10. Lai, C.; Huang, F.L.; Zeng, G.M.; Huang, D.L.; Qin, L.; Cheng, M.; Chen, L. Fabrication of novel magnetic MnFe<sub>2</sub>O<sub>4</sub>/bio-char composite and heterogeneous photo-Fenton degradation of tetracycline in near neutral pH. *Chemosphere* **2019**, *224*, 910–921. [[CrossRef](#)]
11. Wu, X.P.; Nan, Z.D. Degradation of rhodamine B by a novel Fe<sub>3</sub>O<sub>4</sub>/SiO<sub>2</sub> double-mesoporous-shelled hollow spheres through photo-Fenton process. *Mater. Chem. Phys.* **2019**, *227*, 302–312. [[CrossRef](#)]
12. Deng, Y.Y.; Wu, Y.N.; Chen, G.Q.; Zheng, X.L.; Dai, M.; Peng, C.S. Metal-organic framework membranes: Recent development in the synthesis strategies and their application in oil-water separation. *Chem. Eng. J.* **2021**, *405*, 127004. [[CrossRef](#)]
13. Liang, Z.B.; Qu, C.; Guo, W.H.; Zou, R.Q.; Xu, Q. Pristine Metal-Organic Frameworks and their Composites for Energy Storage and Conversion. *Adv. Mater.* **2018**, *30*, e1702891. [[CrossRef](#)] [[PubMed](#)]
14. Yu, H.H.; Fan, M.Y.; Liu, Q.; Su, Z.M.; Li, X.; Pan, Q.Q.; Hu, X.L. Two Highly Water-Stable Imidazole-Based Ln-MOFs for Sensing Fe<sup>3+</sup>, Cr<sub>2</sub>O<sub>7</sub><sup>2-</sup>/CrO<sub>4</sub><sup>2-</sup> in a Water Environment. *Inorg. Chem.* **2020**, *59*, 2005–2010. [[CrossRef](#)] [[PubMed](#)]
15. Cheng, M.; Lai, C.; Liu, Y.; Zeng, G.M.; Huang, D.L.; Zhang, C.; Xiong, W.P. Metal-organic frameworks for highly efficient heterogeneous Fenton-like catalysis. *Coord. Chem. Rev.* **2018**, *368*, 80–92. [[CrossRef](#)]
16. Uthappa, U.T.; Sriram, G.; Arvind, O.R.; Kumar, S.; Ho-Young-Jung Neelgund, G.M.; Kurkuri, M.D. Engineering MIL-100(Fe) on 3D porous natural diatoms as a versatile high performing platform for controlled isoniazid drug release, Fenton's catalysis for malachite green dye degradation and environmental adsorbents for Pb<sup>2+</sup> removal and dyes. *Appl. Surf. Sci.* **2020**, *528*, 146974. [[CrossRef](#)]
17. Wu, Q.S.; Yang, H.P.; Kang, L.; Gao, Z.; Ren, F.F. Fe-based metal-organic frameworks as Fenton-like catalysts for highly efficient degradation of tetracycline hydrochloride over a wide pH range: Acceleration of Fe(II)/Fe(III) cycle under visible light irradiation. *Appl. Catal. B-Environ.* **2020**, *263*, 118282. [[CrossRef](#)]
18. Lv, X.Y.; Jin, G.P.; Yuan, D.K.; Ding, Y.F.; Long, P.X. Improving generation of H<sub>2</sub>O<sub>2</sub> and center dot OH at copper hexacyanocobaltate/graphene/ITO composite electrode for degradation of levofloxacin in photo-electro-Fenton process. *Environ. Sci. Pollut. Res.* **2021**, *28*, 17636–17647. [[CrossRef](#)]
19. Chen, L.Y.; Wang, H.F.; Li, C.X.; Xu, Q. Bimetallic metal-organic frameworks and their derivatives. *Chem. Sci.* **2020**, *11*, 5369–5403. [[CrossRef](#)]
20. Lu, X.F.; Gu, L.F.; Wang, J.W.; Wu, J.X.; Liao, P.Q.; Li, G.R. Bimetal-Organic Framework Derived CoFe<sub>2</sub>O<sub>4</sub>/C Porous Hybrid Nanorod Arrays as High-Performance Electrocatalysts for Oxygen Evolution Reaction. *Adv. Mater.* **2017**, *29*, 1604437. [[CrossRef](#)]
21. Tang, J.T.; Wang, J.L. MOF-derived three-dimensional flower-like FeCu@C composite as an efficient Fenton-like catalyst for sulfamethazine degradation. *Chem. Eng. J.* **2019**, *375*, 122007. [[CrossRef](#)]
22. Sun, Q.; Liu, M.; Li, K.Y.; Han, Y.T.; Zuo, Y.; Chai, F.F.; Guo, X.W. Synthesis of Fe/M(M = Mn, Co, Ni) bimetallic metal organic frameworks and their catalytic activity for phenol degradation under mild conditions. *Inorg. Chem. Front.* **2017**, *4*, 144–153. [[CrossRef](#)]
23. Li, C.X.; Chen, C.B.; Lu, J.Y.; Cui, S.; Li, J.; Liu, H.Q.; Zhang, F. Metal organic framework-derived CoMn<sub>2</sub>O<sub>4</sub> catalyst for heterogeneous activation of peroxydisulfate and sulfanilamide degradation. *Chem. Eng. J.* **2018**, *337*, 101–109. [[CrossRef](#)]
24. Wang, Q.; Ma, Y.; Xing, S.T. Comparative study of Cu-based bimetallic oxides for Fenton-like degradation of organic pollutants. *Chemosphere* **2018**, *203*, 450–456. [[CrossRef](#)] [[PubMed](#)]

25. Wei, Y.H.; Wang, C.R.; Liu, D.; Jiang, L.X.; Chen, X.Y.; Li, H.Y.; Zhang, F.L. Photo-catalytic oxidation for pyridine in circumneutral aqueous solution by magnetic Fe-Cu materials activated H<sub>2</sub>O<sub>2</sub>. *Chem. Eng. Res. Des.* **2020**, *163*, 1–11. [[CrossRef](#)]
26. Tang, J.T.; Wang, J.L. Fenton-like degradation of sulfamethoxazole using Fe-based magnetic nanoparticles embedded into mesoporous carbon hybrid as an efficient catalyst. *Chem. Eng. J.* **2018**, *351*, 1085–1094. [[CrossRef](#)]
27. Luo, X.L.; Hu, H.T.; Pan, Z.; Pei, F.; Qian, H.M.; Miao, K.K.; Feng, G.D. Efficient and stable catalysis of hollow Cu<sub>9</sub>S<sub>5</sub> nanospheres in the Fenton-like degradation of organic dyes. *J. Hazard. Mater.* **2020**, *396*, 122735. [[CrossRef](#)]
28. Chen, J.X.; Xing, Z.; Han, J.; Su, M.; Li, Y.H.; Lu, A.D. Enhanced degradation of dyes by Cu-Co-Ni nanoparticles loaded on amino-modified octahedral metal-organic framework. *J. Alloy. Compd.* **2020**, *834*, 155106. [[CrossRef](#)]
29. Qin, L.; Ru, R.; Mao, J.W.; Meng, Q.; Fan, Z.; Li, X.; Zhang, G.L. Assembly of MOFs/polymer hydrogel derived Fe<sub>3</sub>O<sub>4</sub>-CuO@hollow carbon spheres for photochemical oxidation: Freezing replacement for structural adjustment. *Appl. Catal. B-Environ.* **2020**, *269*, 118754. [[CrossRef](#)]
30. Wu, Z.L.; Wang, Y.P.; Xiong, Z.K.; Ao, Z.M.; Pu, S.Y.; Yao, G.; Lai, B. Core-shell magnetic Fe<sub>3</sub>O<sub>4</sub>@Zn/Co-ZIFs to activate peroxymonosulfate for highly efficient degradation of carbamazepine. *Appl. Catal. B-Environ.* **2020**, *277*, 119136. [[CrossRef](#)]
31. Zuo, S.J.; Jin, X.M.; Wang, X.W.; Lu, Y.H.; Zhu, Q.; Wang, J.W.; Wang, J. Sandwich structure stabilized atomic Fe catalyst for highly efficient Fenton-like reaction at all pH values. *Appl. Catal. B-Environ.* **2021**, *282*, 119551. [[CrossRef](#)]
32. Pang, J.B.; Fu, F.L.; Li, W.B.; Zhu, L.J.; Tang, B. Fe-Mn binary oxide decorated diatomite for rapid decolorization of methylene blue with H<sub>2</sub>O<sub>2</sub>. *Appl. Surf. Sci.* **2019**, *478*, 54–61. [[CrossRef](#)]
33. Liu, X.H.; Yang, C.Y.; Wang, Y.Q.; Guo, Y.L.; Guo, Y.; Lu, G.Z. Effect of the diatomite pretreatment on the catalytic performance of TS-1/diatomite for toluene hydroxylation by H<sub>2</sub>O<sub>2</sub> in fixed-bed reactor. *Chem. Eng. J.* **2014**, *243*, 192–196. [[CrossRef](#)]
34. Dai, D.; Liang, H.; He, D.S.; Potgieter, H.; Li, M. Mn-doped Fe<sub>2</sub>O<sub>3</sub>/diatomite granular composite as an efficient Fenton catalyst for rapid degradation of an organic dye in solution. *J. Sol-Gel Sci. Technol.* **2021**, *97*, 329–339. [[CrossRef](#)]
35. Hu, H.; Zhang, H.X.; Chen, Y.; Chen, Y.J.; Zhuang, L.; Ou, H.S. Enhanced photocatalysis degradation of organophosphorus flame retardant using MIL-101(Fe)/persulfate: Effect of irradiation wavelength and real water matrixes. *Chem. Eng. J.* **2019**, *368*, 273–284. [[CrossRef](#)]
36. Rostamnia, S.; Alamgholiloo, H.; Liu, X. Pd-grafted open metal site copper-benzene-1,4-dicarboxylate metal organic frameworks (Cu-BDC MOF's) as promising interfacial catalysts for sustainable Suzuki coupling. *J. Colloid Interface Sci.* **2016**, *469*, 310–317. [[CrossRef](#)] [[PubMed](#)]
37. Tang, J.; Wang, J. Iron-copper bimetallic metal-organic frameworks for efficient Fenton-like degradation of sulfamethoxazole under mild conditions. *Chemosphere* **2020**, *241*, 125002. [[CrossRef](#)]
38. Huang, X.; Wei, J.Y.; Jiang, X.; Nan, Z.D. FeS<sub>2</sub>/SiO<sub>2</sub> mesoporous hollow spheres formation and catalytic properties in the Fenton reaction. *Mater. Lett.* **2020**, *277*, 128408. [[CrossRef](#)]
39. Wu, Q.S.; Siddique, M.S.; Guo, Y.L.; Wu, M.; Yang, Y.K.; Yang, H.P. Low-crystalline bimetallic metal-organic frameworks as an excellent platform for photo-Fenton degradation of organic contaminants: Intensified synergism between hetero-metal nodes. *Appl. Catal. B-Environ.* **2021**, *286*, 119950. [[CrossRef](#)]
40. Zhang, H.J.; Zhou, C.; Zeng, H.X.; Deng, L.; Shi, Z. Can Cu<sub>2</sub>ZnSnS<sub>4</sub> nanoparticles be used as heterogeneous catalysts for sulfadiazine degradation? *J. Hazard. Mater.* **2020**, *395*, 122613. [[CrossRef](#)]
41. Wang, Q.; Wang, P.; Xu, P.; Li, Y.; Duan, J.J.; Zhang, G.S.; Zhang, W. Visible-light-driven photo-Fenton reactions using Zn<sub>1</sub>-1.5xFexS/g-C<sub>3</sub>N<sub>4</sub> photocatalyst: Degradation kinetics and mechanisms analysis. *Appl. Catal. B-Environ.* **2020**, *266*, 118653. [[CrossRef](#)]
42. Rej, S.; Bisetto, M.; Naldoni, A.; Fornasiero, P. Well-defined Cu<sub>2</sub>O photocatalysts for solar fuels and chemicals. *J. Mater. Chem. A* **2021**, *9*, 5915–5951. [[CrossRef](#)]
43. Zhang, Y.; Zhou, J.; Chen, X.; Wang, L.; Cai, W. Coupling of heterogeneous advanced oxidation processes and photocatalysis in efficient degradation of tetracycline hydrochloride by Fe-based MOFs: Synergistic effect and degradation pathway. *Chem. Eng. J.* **2019**, *369*, 745–757. [[CrossRef](#)]
44. Chen, Y.Y.; Ma, Y.L.; Yang, J.; Wang, L.Q.; Lv, J.M.; Ren, C.J. Aqueous tetracycline degradation by H<sub>2</sub>O<sub>2</sub> alone: Removal and transformation pathway. *Chem. Eng. J.* **2017**, *307*, 15–23. [[CrossRef](#)]
45. Xin, S.S.; Liu, G.C.; Ma, X.H.; Gong, J.X.; Ma, B.R.; Yan, Q.H.; Xin, Y.J. High efficiency heterogeneous Fenton-like catalyst biochar modified CuFeO<sub>2</sub> for the degradation of tetracycline: Economical synthesis, catalytic performance and mechanism. *Appl. Catal. B-Environ.* **2021**, *280*, 119386. [[CrossRef](#)]
46. Jiang, J.J.; Gao, J.Y.; Niu, S.; Wang, X.Y.; Li, T.R.; Liu, S.D.; Dong, S.S. Comparing dark- and photo-Fenton-like degradation of emerging pollutant over photo-switchable Bi<sub>2</sub>WO<sub>6</sub>/CuFe<sub>2</sub>O<sub>4</sub>: Investigation on dominant reactive oxidation species. *J. Environ. Sci.* **2021**, *106*, 147–160. [[CrossRef](#)] [[PubMed](#)]
47. Zhang, X.; Yao, Z.P.; Zhou, Y.; Zhang, Z.R.; Lu, G.F.; Jiang, Z.H. Theoretical guidance for the construction of electron-rich reaction microcenters on C-O-Fe bridges for enhanced Fenton-like degradation of tetracycline hydrochloride. *Chem. Eng. J.* **2021**, *411*, 128535. [[CrossRef](#)]